Detecting topological invariants and revealing topological phase transitions in discrete-time photonic quantum walks

Xiaoping Wang,[1,2] Lei Xiao,[1,2] Xingze Qiu,[3,4] Kunkun Wang,[1,2] Wei Yi,[3,4,*] and Peng Xue[1,2,5,†]

[1]*Beijing Computational Science Research Center, Beijing 100084, China*

[2]*Department of Physics, Southeast University, Nanjing 211189, China*

[3]*Key Laboratory of Quantum Information, University of Science and Technology of China, CAS, Hefei 230026, China*

[4]*Synergetic Innovation Center in Quantum Information and Quantum Physics, University of Science and Technology of China, CAS, Hefei 230026, China*

[5]*State Key Laboratory of Precision Spectroscopy, East China Normal University, Shanghai 200062, China*

(Received 5 May 2018; published 20 July 2018)

We experimentally investigate topological phenomena in one-dimensional discrete-time photonic quantum walks using a combination of methods. We first detect winding numbers of the quantum walk by directly measuring the average chiral displacement, which oscillates around quantized winding numbers for finite-step quantum walks. Topological phase transitions can be identified as changes in the center of oscillation of the measured chiral displacement. The position of topological phase transition is then confirmed by measuring the moments of the walker probability distribution. Finally, we observe localized edge states at the boundary of regions with different winding numbers. We also confirm the robustness of edge states against chiral-symmetry-preserving disorder.

DOI: 10.1103/PhysRevA.98.013835

I. INTRODUCTION

The quantum walk [1–3] is a versatile and highly controllable platform for quantum algorithms [4–7] and quantum simulations [8–13]. In recent years, quantum walks have been realized experimentally in a wide range of physical systems such as nuclear magnetic resonance [14–16], trapped atoms [17–19] and ions [20,21], linear optics [22–28], and integrated optics [29–31]. A particularly intriguing study here is the Floquet topological phases (FTPs) in discrete-time quantum walks, which have been experimentally implemented, for example, using photons in interferometric network [10–13,32–34].

Topological phases exhibit remarkable properties, and have stimulated extensive research interest in modern physics [35,36]. In contrast to conventional phases of matter which are characterized by symmetry properties and local order parameters, topological phases are typically parametrized by integer-valued topological invariants [35–40]. As integers cannot change continuously, a necessary consequence is the emergence of exotic phenomena, such as topological edge states, at the boundary between regions with different topological invariants. Whereas the existence of robust topological edge states localized at a boundary constitute a smoking-gun evidence for topological phenomena, direct detections of topological invariants in the bulk have been made possible by probing losses from the system [41]. However, the method of detecting topological invariants in nonunitary quantum walks via loss [13] cannot be extended to the case of unitary quantum walks. Recently, Cardano *et al.* [11] have shown that in chiral one-dimensional unitary Floquet systems, the average chiral displacement of a particle's wave packet becomes quantized and proportional to the winding number in the long-time limit. Further, the same group has demonstrated that statistical moments of the unitary quantum-walk dynamics can also be used to characterize topological phase transitions in the bulk.

In this work, we report an experimental characterization of topological phenomena in discrete-time photonic quantum walks in one dimension. Adopting a split-step quantum walk of single photons, we measure the chiral displacement and the statistical moments of the dynamics. While in the long-time limit, chiral displacement should be quantized and converge to the bulk winding numbers, we show that for the experimentally achievable finite-step quantum-walk dynamics, the chiral displacement exhibits oscillatory behavior centered around the bulk winding numbers. Topological phase transitions can be identified as changes in the center of oscillation of the measured chiral displacement, which is consistent with topological phase boundaries deduced from the statistical-moment measurements. Finally, we confirm the measured topological invariants by direct observations of robust topological edge states at the boundary of regions with distinct winding numbers. By a systematic study of topological phenomena in discrete-time split-step quantum walks, our results lay the foundation for future studies of topological phenomena in multistep quantum walks, where higher winding numbers exist.

Compared to the previous experiments in [10,11], the physical system is different. The walker is encoded in the spatial modes of single photons, instead of the orbital angular momentum of light. In other words, we employ the "real" position space, instead of "abstract" position space, i.e., the transverse modes of the light beam. Furthermore, it is easy

*wyiz@ustc.edu.cn

†gnep.eux@gmail.com

to realize inhomogeneous quantum walks in our experimental setup. Thus, we are able to observe topological edge states and their robustness to symmetry-preserving disorder.

The paper is organized as follows. In Sec. II, we introduce the experimentally realized split-step quantum walk, and characterize its topological properties using winding numbers. We discuss the theoretical aspects of chiral displacement and statistical moments of the split-step quantum walk in Sec. III. In Sec. IV, we present our experimental results. We confirm the measured topological invariants by detecting robust topological edge states in Sec. V. Finally, we summarize in Sec. VI.

II. TOPOLOGICAL INVARIANTS FOR SPLIT-STEP QUANTUM WALKS

We start from a split-step quantum walk governed by the unitary Floquet operators,

$$\begin{aligned} U_1 &= R(\theta_1/2)SR(\theta_2)SR(\theta_1/2), \\ U_2 &= R(\theta_2/2)SR(\theta_1)SR(\theta_2/2), \end{aligned} \tag{1}$$

where $R(\theta) = \sum_x |x\rangle\langle x| \otimes e^{-i\theta(x)\sigma_y}$ is the position-dependent coin rotation, σ_y is a Pauli operator, and $S = \sum_x |x+1\rangle\langle x| \otimes |1\rangle\langle 1| + |x-1\rangle\langle x| \otimes |0\rangle\langle 0|$ is the conditional position shift operator. Here, x denotes the position of the walker and $\{|0\rangle, |1\rangle\}$ are two orthogonal coin states. As the system has translation invariance, we can adopt the Fourier transformation $|x\rangle = \frac{1}{\sqrt{N}}\sum_k e^{-ikx}|k\rangle$, where N is the total site number, and rewrite the Floquet operators U_1 and U_2 with $R(\theta) = e^{-i\theta\sigma_y}$ and $S = e^{ik\sigma_z}$. The Floquet operators U_1 and U_2 have chiral symmetry with the symmetry operator $\Gamma = \sigma_x$, i.e., $\Gamma U_{1,2}\Gamma = U_{1,2}^{-1}$.

We then introduce the effective Hamiltonian $H_{\text{eff}}(k) = E_k \mathbf{n}_\mathbf{k} \cdot \sigma$ through $U_1 = e^{-iH_{\text{eff}}}$ with E_k the quasienergy dispersion of FTPs, σ the Pauli vector, and $\mathbf{n}$ indicating the direction of the spinor eigenstate at each momentum $-\pi < k \leqslant \pi$. It is straightforward to derive [8,10–13]

$$\begin{aligned} \cos E_k &= \cos\theta_1 \cos\theta_2 \cos 2k - \sin\theta_1 \sin\theta_2, \\ n_x &= 0, \\ n_y &= \frac{1}{\sin E_k}(\cos\theta_2 \sin\theta_1 \cos 2k + \cos\theta_1 \sin\theta_2), \\ n_z &= -\frac{1}{\sin E_k}\cos\theta_2 \sin 2k, \\ n_y^2 + n_z^2 &= 1. \end{aligned} \tag{2}$$

The topological invariant of the FTP is the winding number defined as

$$\nu_1 = \frac{1}{2\pi}\oint dk \left(\mathbf{n} \times \frac{\partial \mathbf{n}}{\partial k}\right)_x. \tag{3}$$

The winding number above is the number of times the vector $\mathbf{n}$ which lies in the y-x plane, winds around the x axis as k varies through the first Brillouin zone. Similarly, we can define ν_2 for the Floquet operator U_2. Note that the winding number Eq. (3) is defined through the spinor eigenvectors of U_1. This is equivalent to the definition through the spin eigenvectors of the corresponding effective Hamiltonian $H_{\text{eff}}(k)$. We also

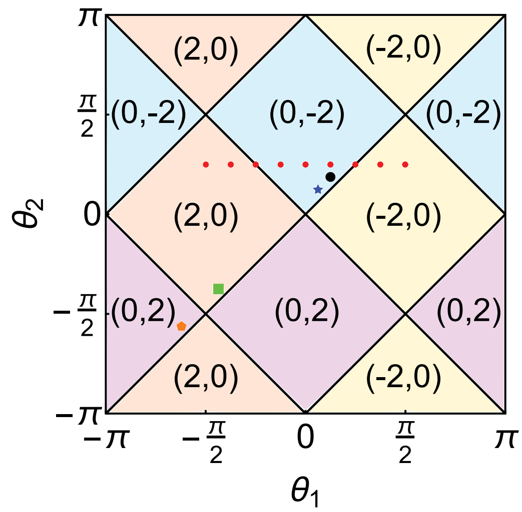

FIG. 1. Phase diagrams of the split-step quantum walk governed U_1. Different topological phases are characterized by the winding numbers (ν_1, ν_2). Black solid lines mark the topological phase boundaries. Nine red dots indicate the coin parameters for detecting the topological invariants. The other colored symbols indicate the coin parameters for observing the topological edge states.

define [42]

$$(\nu_0, \nu_\pi) := \left(\frac{\nu_1 + \nu_2}{2}, \frac{\nu_1 - \nu_2}{2}\right), \tag{4}$$

which are directly related to edge states at the boundaries with quasienergies 0 and π, respectively. Specifically, the number of edge states with quasienergy 0 (π) should be equal to the difference in the winding numbers ν_0 (ν_π) on either side of the boundary. In Fig. 1, we show the phase diagram on the $\theta_1 - \theta_2$ plane with topological invariants (ν_1, ν_2).

III. CHIRAL DISPLACEMENTS AND STATISTICAL MOMENTS OF QUANTUM WALKS

In this section, we introduce the average chiral displacement and the statistical moments of unitary quantum walks. Consider a general initial state of the walker-coin system as $|\Psi_0\rangle = |x = 0\rangle \otimes |\psi_0\rangle$, where $|\psi_0\rangle$ represents the coin state. At any given time step $t > 0$, we have $|\Psi_t\rangle = U_1^t|\Psi_0\rangle$, and the probability of measuring the walker at position x is

$$p(x,t) = \langle\Psi_t|x\rangle\langle x| \otimes \mathbb{1}_c|\Psi_t\rangle, \tag{5}$$

where $\mathbb{1}_c = |0\rangle\langle 0| + |1\rangle\langle 1|$ is the identity matrix for the coin space.

The average chiral displacement is defined as [11]

$$C(t) = \langle\Gamma x\rangle = \frac{\sum_x \langle\Psi_t|x\rangle\langle x| \otimes \Gamma|\Psi_t\rangle}{\sum_x \langle\Psi_t|x\rangle\langle x| \otimes \mathbb{1}_c|\Psi_t\rangle}, \tag{6}$$

which quantifies the relative shift between the two projections of the states onto the eigenstates of the chiral operator Γ. The winding number can be simply achieved by the scaled average chiral displacement of the walker $-2C(t)$, whose location is consistent with topological phase boundaries.

The j^{th} statistical moment of this distribution is given by $M_j(t) = \langle x^j\rangle_t = \sum_x x^j p(x,t)$ [10]. In particular, we write the first and second moments in the momentum space as [10]

$$M_1(t) = \int_{-\pi}^{\pi} \frac{dk}{2\pi} \langle\psi_0|U^{\dagger t}\left(-i\frac{d}{\mathrm{d}k}\right)U^t|\psi_0\rangle \tag{7}$$

and

$$M_2(t) = \int_{-\pi}^{\pi} \frac{dk}{2\pi} \langle\psi_0|U^{\dagger t}\left(-i\frac{d}{dk}\right)^2 U^t|\psi_0\rangle. \tag{8}$$

Specifically, we have $U_1 = \cos E_k\sigma_0 - i\sin E_k(\hat{\mathbf{n}}_k\cdot\sigma) \Rightarrow U_1^t = \cos(E_kt)\sigma_0 - i\sin(E_kt)(\hat{\mathbf{n}}_k\cdot\sigma)$, where $\hat{\mathbf{n}}_k = \mathbf{n}_k/\sin E_k$ and $\cos E_k = n_0$. It is then straightforward to derive [10]

$$\begin{aligned} \frac{M_1(t)}{t} &= \langle\Psi_0|(\sigma_y-\sigma_z)|\Psi_0\rangle\int_{-\pi}^{\pi}\frac{dk}{2\pi}v_k^2 + O(1/t),\\ \frac{M_2(t)}{t^2} &= \int_{-\pi}^{\pi}\frac{dk}{2\pi}v_k^2 + O(1/t^2), \\ \int_{-\pi}^{\pi}\frac{dk}{2\pi}v_k^2 &= \int_{-\pi}^{\pi}\frac{dk}{2\pi}\left(\frac{dE_k}{dk}\right)^2 = \int_{-\pi}^{\pi}\frac{dk}{2\pi}\frac{1}{1-n_0^2}\left(\frac{dn_0}{dk}\right)^2, \end{aligned} \tag{9}$$

where $v_k = \frac{dE_k}{dk}$ is the group velocity. At the topological phase boundary, the bulk gap closes at certain points in the momentum space, and the corresponding $n_0(k)$ at these momenta approaches zero. This gives rise to the slope discontinuity, as well as a peak structure of the first and second moments near the phase boundary [10]. Thus the probability distribution moments of the walker position can be used as direct indicators of the topological quantum transitions in a long-time limit.

IV. EXPERIMENTAL REALIZATION OF MULTISTEP NONUNITARY QUANTUM WALKS

For a single-photon quantum walk, the coin states are represented by the horizontal $|H\rangle$ and vertical $|V\rangle$ polarization states of the photons, and the walker states are encoded in their spatial modes. As shown in Fig. 2, a pair of photons is generated via type-I spontaneous parametric downconversion. With one photon serving as a trigger, the other photon is projected into the state $|+\rangle = (|H\rangle + |V\rangle)/\sqrt{2}$ with a polarizing beamsplitter (PBS) and a half-wave plate (HWP) heralded by the trigger photon, and is then sent to the quantum-walk interferometric setup. We implement the coin operator $R(\theta)$ via two HWPs and the shift operator S via a beam displacer whose optical axis is cut so that the photons in $|V\rangle$ are directly transmitted and those in $|H\rangle$ undergo a lateral displacement into a neighboring mode [13]. After passing through the quantum-walk interferometric network, we apply a projective measurement on the photons with the basis $\{|+\rangle, |-\rangle\}$, and $|\pm\rangle$ are the eigenstates of the chiral operator Γ. The projective measurement is realized by a HWP at 22.5° following by a PBS. After passing through the HWP, the photons in the state $|-\rangle$ are projected into $|V\rangle$ and then reflected by the PBS, while the photons in $|+\rangle$ are projected into $|H\rangle$ and transmitted. Finally, for a t-step quantum walk, we perform coincidence measurements on both reflected and transmitted photons at each position successively up to t by single-photon avalanche photodiodes (APDs).

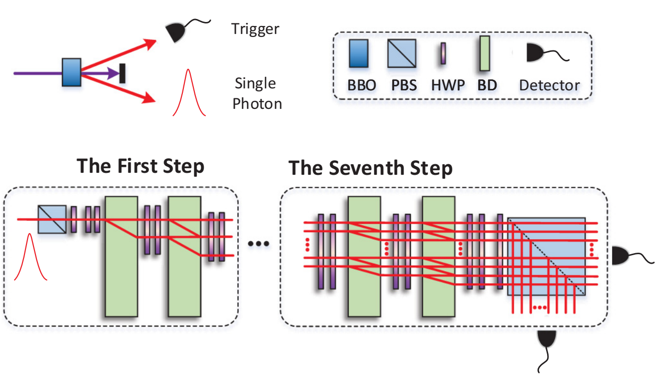

FIG. 2. Experimental setup. The photon pair is created via spontaneous parametric downconversion. One photon serves as a trigger and the other photon is projected into the polarization state $|+\rangle$ with a PBS and a HWP at 22.5°. The coin rotation R is realized by two HWPs with certain setting angles and the conditional position shift operator S is realized by a BD. Finally, the photons are detected by APDs in coincidence with the trigger photons.

Similar to the Zak phase in a quantum walk based on the orbital angular momentum of a light beam [11], the winding number in our system can be detected by measuring the average chiral displacement of the walker initially prepared in $|\Psi_0\rangle = |0\rangle|+\rangle$. We realize seven-step quantum walks with a fixed $\theta_2 = \pi/4$ and varying θ_1 along the red dotted lines in the phase diagrams. The experimental results of the scaled average chiral displacements are shown in Fig. 3(a) for evolution operator U_1 (those for U_2 are not shown). The results agree well with the numerical simulations of seven-step quantum walks and demonstrate plateaux close to quantized value ν_1 calculated from infinite-step quantum walks. For completeness we also show results predicted for 51 steps in Fig. 3(b), and the asymptotic long-time limit. We note here that, although both theoretical and experimental data oscillate, as few as seven steps are enough to have a clear detection of winding numbers.

Now we demonstrate topological phase transitions between FTPs with different topological invariants by probing statistical moments of the walker. Experimentally, the moment is evaluated from the spatial distribution of the photons at the last step. In Fig. 4, we plot the measured values of $M_1(t)/t$ of the quantum walk governed by U_1 with a fixed $\theta_2 = \pi/4$ and varying θ_1 up to seven steps and those predicted theoretically for 51 steps. The coin parameter scanned along the red

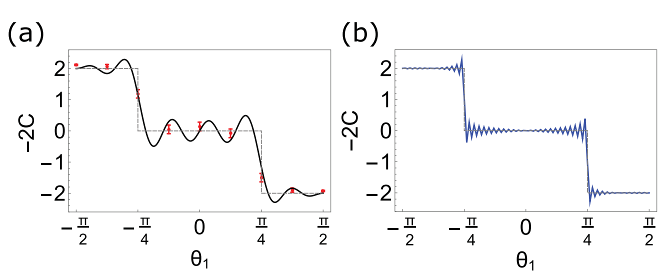

FIG. 3. (a) Scaled chiral displacement of the quantum walk governed by U_1 with a fixed $\theta_2 = \pi/4$ and varying θ_1 as indicated by the nine red dots in the phase diagram. The solid curve represents the theoretical result for the seven-step quantum walk and the experimental results are shown by dots. The dashed curve indicates the expected results of infinite-step quantum walks. (b) Theoretical predictions of the scaled chiral displacement in the long-time limit ($t = 51$). Experimental errors are due to photon-counting statistics.

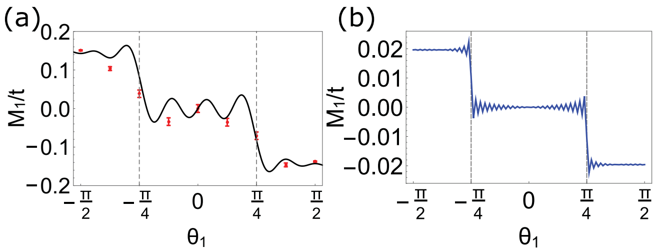

FIG. 4. (a) Statistical moments $M_1(t)/t$ of the walker position distribution of the seven-step quantum walk governed by U_1 with a fixed $\theta_2 = \pi/4$ and varying θ_1 as indicated by nine red dots in the phase diagram. The solid curve represents the theoretical result for the seven-step quantum walk and the experimental results are shown by dots. The dashed line indicates where topological quantum transition occurs. (b) Theoretical predictions of $M_1(t)/t$ in the long-time limit ($t = 51$).

dotted lines in the phase diagrams. Similar to the behavior of the scaled average chiral displacement, both theoretical predictions in the long-time limit and the experimental results oscillate and we find good agreement between experimental results and theoretical predictions with the same evolution time.

In Fig. 5, we confirm the topological phase boundaries, signaled by jumps of the measured topological invariants, by probing the second statistical moments $M_2(t)/t^2$. The measured $M_2(t)/t^2$ exhibits anomalies near the topological phase transitions. The emergence of an abrupt slope variation at $\pm\pi/4$ can be appreciated and the observed nonanalyticity is a signature of the underlying quantum transition. We find reasonable agreement between experimental results and theoretical predictions. The differences between the experimental results and the theoretical ones are due to experimental imperfections, especially decoherence.

Here, we show that much of the discrepancy between the experimental results and the theoretical ones is attributed to decoherence. In our experiment, the major decoherence is dephasing caused by the misalignment between BDs. To simplify our estimation, we assume the dephasing rate η is constant. The density matrix ρ_t evolves according to [13]

$$\begin{aligned}
\rho_{t+1}^{(1)} &= SR\left(\frac{\theta_1}{2}\right)\rho_t R^\dagger\left(\frac{\theta_1}{2}\right)S^\dagger,\\
\rho_{t+1}^{(2)} &= \eta\rho_{t+1}^{(1)} + (1-\eta)(\mathbb{1}_\mathrm{w}\otimes\sigma_z)\rho_{t+1}^{(1)}(\mathbb{1}_\mathrm{w}\otimes\sigma_z)^\dagger,\\
\rho_{t+1}^{(3)} &= SR(\theta_2)\rho_{t+1}^{(2)}R^\dagger(\theta_2)S^\dagger,\\
\rho_{t+1}^{(4)} &= \eta\rho_{t+1}^{(3)} + (1-\eta)(\mathbb{1}_\mathrm{w}\otimes\sigma_z)\rho_{t+1}^{(3)}(\mathbb{1}_\mathrm{w}\otimes\sigma_z)^\dagger,\\
\rho_{t+1} &= R\left(\frac{\theta_1}{2}\right)\rho_{t+1}^{(4)}R\left(\frac{\theta_1}{2}\right).
\end{aligned} \tag{10}$$

For seven-step quantum walks under U_1, the effect of dephasing on the polarizations of the photons gives rise to the quantum-to-classical transition, and renders the probability distribution of the walker Gaussian-like in the long-time limit. In Fig. 5(c), we show the numerically simulated average chiral displacement for seven-step quantum walks with different dephasing rates, which qualitatively explains the small discrepancy between the experimental results and the numerically ones in Fig. 5(a).

V. TOPOLOGICAL EDGE STATES AND THEIR ROBUSTNESS AGAINST DISORDER

To confirm the topological properties of the split-step quantum walk, we create regions with distinct topological invariants and probe the existence of edge states via localized probability distribution at the boundaries between two regions. The boundaries are created by making the coin parameters spatially inhomogeneous, such as (θ_1^l, θ_2^l) for the left region $x < 0$ and (θ_1^r, θ_2^r) for the left region $x \geqslant 0$. These spatially inhomogeneous coin rotations in our experiment are realized via HWPs individually inserted in the special paths. To observe edge states, we fix the coin parameters for the right region $(\theta_1^r, \theta_2^r) = (\pi/8, 3\pi/16)$, which belongs to the topological phase with bulk topological invariants $(\nu_0, \nu_\pi) = (-1, 1)$ $[(\nu_1, \nu_2) = (0, -2)]$.

First, we choose the coin parameters for the left region $(\theta_1^l, \theta_2^l) = (\pi/16, \pi/8)$, which belongs to the topological phase with the same bulk topological invariants compared to the right region. No edge state is expected, which is confirmed by the experimental results. In Fig. 6(a), the distribution of the quantum walk governed by U_1 up to five steps shows ballistic behavior and no localization is observed. We also show the comparison of the measured and predicted probabilities after the fifth step.

Second, we choose the coin parameters for the left region $(\theta_1^l, \theta_2^l) = (-7\pi/16, -3\pi/8)$, which belongs to the topological phase with the bulk topological invariants $(\nu_0, \nu_\pi) = (1, 1)$ $[(\nu_1, \nu_2) = (2, 0)]$. As the topological invariants ν_0 for the left and right regions are different, we expect to observe the

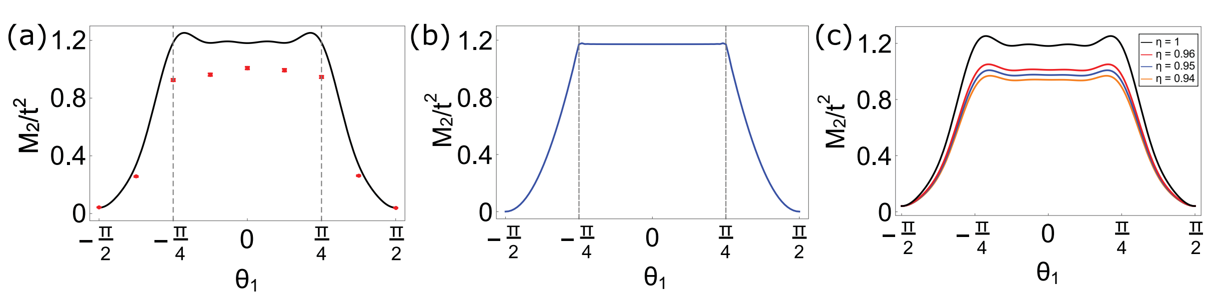

FIG. 5. (a) Statistical moments $M_2(t)/t^2$ of the walker position distribution for the quantum walk governed by U_1 with a fixed $\theta_2 = \pi/4$ and varying θ_1 up to seven steps. Error bars are smaller than symbol size. (b) Theoretical predictions of $M_2(t)/t^2$ in the long-time limit ($t = 51$). (c) Simulated $M_2(t)/t^2$ for the seven-step quantum walk under dephasing, for the protocol U_1.

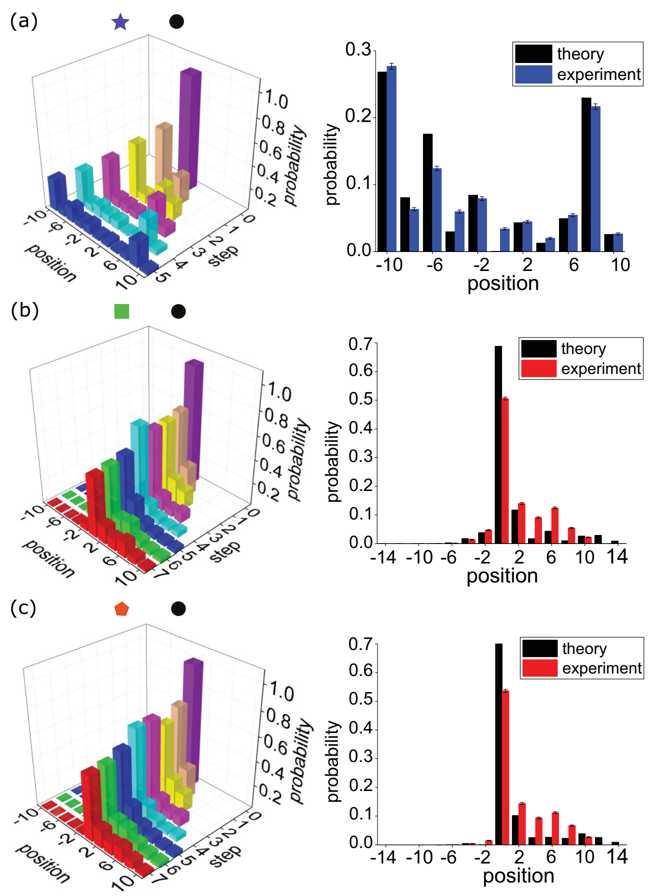

FIG. 6. Experimental observation of topological edge states in the inhomogeneous quantum walk governed by U_1. (Left column) The measured probability distributions with fixed coin parameters for the right region $(\theta_1^r,\theta_2^r)=(\pi/8,3\pi/16)$ and varying those for the left regions indicated by the symbols in the phase diagram, such as $(\theta_1^l,\theta_2^l)=(\pi/16,\pi/8)$ (a), $(\theta_1^l,\theta_2^l)=(-7\pi/16,-3\pi/8)$ (b), and $(\theta_1^l=-5\pi/8,\theta_2^l=-9\pi/16)$ (c). (Right column) The comparison between experimental results and theoretical predictions of the probability distribution of the quantum walk after the last step.

topological edge states near the boundary. In Fig. 6(b), a localized distribution is shown and the probability of the walker $P(0)$ is clearly enhanced for each step up to seven steps, which confirms the existence of the edge states.

Third, we choose the coin parameters for the left region $(\theta_1^l,\theta_2^l)=(-5\pi/8,-9\pi/16)$, which belongs to the topological phase with the bulk topological invariants $(\nu_0,\nu_\pi)=(1,-1)$ $[(\nu_1,\nu_2)=(0,2)]$. Both topological invariants are different and thus edge states are also expected in this case, which is confirmed by the experimental results shown in Fig. 6(c).

A key feature of topologically nontrivial systems is the robustness of topological properties against small perturbations. We find that the edge states of the split-step quantum walk here is robust against static disorders which is chiral symmetry preserving. We keep the mean values of the coin parameters $(\langle\theta_1^r\rangle,\langle\theta_1^r\rangle)=(\pi/8,3\pi/16)$ and $(\langle\theta_1^l\rangle,\langle\theta_1^l\rangle)=(-7\pi/16,-3\pi/8)$. We implement five-step quantum-walk dynamics governed by the evolution operator U_1 with 10

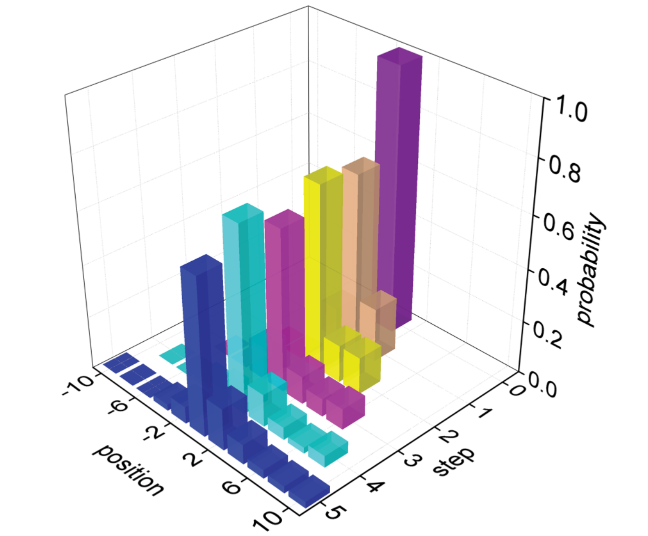

FIG. 7. Edge states are robust against static disorder to the rotations $R(\langle\theta_{1,2}\rangle+\delta\theta)$ and $\delta\theta\in[-\pi/20,\pi/20]$. The measured probability distribution of the quantum walk governed by U_1 with $(\langle\theta_1^r\rangle,\langle\theta_1^r\rangle)=(\pi/8,3\pi/16)$ and $(\langle\theta_1^l\rangle,\langle\theta_1^l\rangle)=(-7\pi/16,-3\pi/8)$ up to five steps.

randomly generated coin rotations $R(\langle\theta_{1,2}\rangle+\delta\theta)$ for each position. The time-independent $\delta\theta$ is unique for each position and chosen from the intervals $[-\pi/20,\pi/20]$. In our experiment, $\delta\theta$ is implemented by manipulating the setting angles of HWPs by small random amounts $\delta\theta$ around the coin parameters (θ_1,θ_2). We then calculate the mean values of the 10 sets of the probabilities of the walker. As shown in Fig. 7, the probability distribution still shows localized behavior and $P(0)$ is obviously enhanced.

VI. DISCUSSION AND CONCLUSION

In summary, we experimentally investigate the topological phenomena in one-dimensional discrete-time quantum walks by directly measuring the average chiral displacement which converges rapidly the winding number in the long-time limit. Furthermore, we reveal topological quantum transitions via measuring the moments of the walker probability distribution, which are consistent with jumps in winding numbers. Finally, we observe the localized edge states on the boundary of two regions with different topological invariants and the robustness of edge states against chiral-symmetry-preserving disorder. Our work shed new light on studies of topological phenomena and their simulations with proper physical systems. Due to the full dynamic control of quantum walk dynamics, the approaches would be applicable to investigate topological phenomena with more complex symmetries or with a higher dimensionality in the future.

ACKNOWLEDGMENTS

This work has been supported by the Natural Science Foundation of China (Grants No. 11474049, No. 11674056, and No. 11522545) and the Natural Science Foundation of Jiangsu Province (Grant No. BK20160024). W.Y. acknowledges support from the National Key R&D Program (Grant No. 2016YFA0301700) and the "Strategic Priority Research Program(B)" of the Chinese Academy of Sciences (Grant No. XDB01030200).

[1] Y. Aharonov, L. Davidovich, and N. Zagury, Quantum random walks, Phys. Rev. A **48**, 1687 (1993).

[2] A. Ambainis, J. Kempe, and A. Rivosh, Coins make quantum walks faster, in *Proceedings of the Sixteenth Annual ACM-SIAM Symposium on Discrete Algorithms, SODA '05* (Society for Industrial and Applied Mathematics, Philadelphia, 2005), pp. 1099–1108.

[3] A. Nayak and A. Vishwanath, Quantum walk on the line, arXiv:quant-ph/0010117.

[4] N. Shenvi, J. Kempe, and K. Birgitta Whaley, Quantum random-walk search algorithm, Phys. Rev. A **67**, 052307 (2003).

[5] J. Kempe, Quantum random walks: An introductory overview, Contemp. Phys. **44**, 307 (2003).

[6] A. Ambainis, Quantum walks and their algorithmic applications, Int. J. Quantum. Inform. **1**, 507 (2003).

[7] A. M. Childs, R. Cleve, E. Deotto, E. Farhi, S. Gutmann, and D. A. Spielman, Exponential algorithmic speedup by a quantum walk, in *Proceedings of the Thirty-Fifth Annual ACM Symposium on Theory of Computing, STOC'03* (ACM, New York, 2003), pp. 59–68.

[8] T. Kitagawa, M. S. Rudner, E. Berg, and E. Demler, Exploring topological phases with quantum walks, Phys. Rev. A **82**, 033429 (2010).

[9] E. Flurin, V. V. Ramasesh, S. Hacohen-Gourgy, L. S. Martin, N. Y. Yao, and I. Siddiqi, Observing Topological Invariants Using Quantum Walks in Superconducting Circuits, Phys. Rev. X **7**, 031023 (2017).

[10] F. Cardano, M. Maffei, F. Massa, B. Piccirillo, C. De Lisio, G. De Filippis, V. Cataudella, E. Santamato, and L. Marrucci, Statistical moments of quantum-walk dynamics reveal topological quantum transitions, Nat. Commun. **7**, 11439 (2016).

[11] F. Cardano, A. D'Errico, A. Dauphin, M. Maffei, B. Piccirillo, C. De Lisio, G. De Filippis, V. Cataudella, E. Santamato, L. Marrucci, M. Lewenstein, and P. Massignan, Detection of Zak phases and topological invariants in a chiral quantum walk of twisted photons, Nat. Commun. **8**, 15516 (2017).

[12] L. Xiao, X. Zhan, Z. H. Bian, K. K. Wang, X. Zhang, X. P. Wang, J. Li, K. Mochizuki, D. Kim, N. Kawakami, W. Yi, H. Obuse, B. C. Sanders, and P. Xue, Observation of topological edge states in parity-time-symmetric quantum walks, Nat. Phys. **13**, 1117 (2017).

[13] X. Zhan, L. Xiao, Z. Bian, K. Wang, X. Qiu, B. C. Sanders, W. Yi, and P. Xue, Detecting Topological Invariants in Nonunitary Discrete-Time Quantum Walks, Phys. Rev. Lett. **119**, 130501 (2017).

[14] J. Du, H. Li, X. Xu, M. Shi, J. Wu, X. Zhou, and R. Han, Experimental implementation of the quantum random-walk algorithm, Phys. Rev. A **67**, 042316 (2003).

[15] C. A. Ryan, M. Laforest, J. C. Boileau, and R. Laflamme, Experimental implementation of discrete time quantum random walk on an NMR quantum information processor, Phys. Rev. A **72**, 062317 (2005).

[16] D. W. Lu, J. D. Biamonte, J. Li, H. Li, T. H. Johnson, V. Bergholm, M. Faccin, Z. Zimborás, R. Laflamme, J. Baugh, and S. Lloyd, Chiral quantum walks, Phys. Rev. A **93**, 042302 (2016).

[17] M. Karski, L. Förster, J.-M. Choi, A. Steffen, W. Alt, D. Meschede, and A. Widera, Quantum walk in position space with single optically trapped atoms, Science **325**, 174 (2009).

[18] M. Genske, W. Alt, A. Steffen, A. H. Werner, R. F. Werner, D. Meschede, and A. Alberti, Electric Quantum Walks with Individual Atoms, Phys. Rev. Lett. **110**, 190601 (2013).

[19] C. Robens, W. Alt, D. Meschede, C. Emary, and A. Alberti, Ideal Negative Measurements in Quantum Walks Disprove Theories Based on Classical Trajectories, Phys. Rev. X **5**, 011003 (2015).

[20] F. Zähringer, G. Kirchmair, R. Gerritsma, E. Solano, R. Blatt, and C. F. Roos, Realization of a Quantum Walk with One and Two Trapped Ions, Phys. Rev. Lett. **104**, 100503 (2010).

[21] H. Schmitz, R. Matjeschk, C. Schneider, J. Glueckert, M. Enderlein, T. Huber, and T. Schaetz, Quantum Walk of a Trapped Ion in Phase Space, Phys. Rev. Lett. **103**, 090504 (2009).

[22] A. Schreiber, K. N. Cassemiro, V. Potoček, A. Gábris, I. Jex, and C. Silberhorn, Decoherence and Disorder in Quantum Walks: From Ballistic Spread to Localization, Phys. Rev. Lett. **106**, 180403 (2011).

[23] T. Kitagawa, M. A. Broome, A. Fedrizzi, M. S. Rudner, E. Berg, I. Kassal, A. Aspuru-Guzik, E. Demler, and A. G. White, Observation of topologically protected bound states in photonic quantum walks, Nat. Commun. **3**, 882 (2012).

[24] P. Xue, H. Qin, B. Tang, and B. C. Sanders, Observation of quasiperiodic dynamics in a one-dimensional quantum walk of single photons in space, New J. Phys. **16**, 053009 (2014).

[25] P. Xue, R. Zhang, H. Qin, X. Zhan, Z. H. Bian, J. Li, and B. C. Sanders, Experimental Quantum-Walk Revival with a Time-Dependent Coin, Phys. Rev. Lett. **114**, 140502 (2015).

[26] Z. H. Bian, J. Li, H. Qin, X. Zhan, R. Zhang, B. C. Sanders, and P. Xue, Realization of Single-Qubit Positive-Operator-Valued Measurement Via a One-Dimensional Photonic Quantum Walk, Phys. Rev. Lett. **114**, 203602 (2015).

[27] P. Xue, R. Zhang, Z. H. Bian, X. Zhan, H. Qin, and B. C. Sanders, Localized state in a two-dimensional quantum walk on a disordered lattice, Phys. Rev. A **92**, 042316 (2015).

[28] Z. H. Bian, J. Li, X. Zhan, J. Twamley, and P. Xue, Experimental implementation of a quantum walk on a circle with single photons, Phys. Rev. A **95**, 052338 (2017).

[29] A. Peruzzo, M. Lobino, J. C. F. Matthews, N. Matsuda, A. Politi, K. Poulios, X.-Q. Zhou, Y. Lahini, N. Ismail, K. Wörhoff, Y. Bromberg, Y. Silberberg, M. G. Thompson, and J. L. O'Brien, Quantum walks of correlated photons, Science **329**, 1500 (2010).

[30] L. Sansoni, F. Sciarrino, G. Vallone, P. Mataloni, A. Crespi, R. Ramponi, and R. Osellame, Two-Particle Bosonic-Fermionic Quantum Walk Via Integrated Photonics, Phys. Rev. Lett. **108**, 010502 (2012).

[31] A. Crespi, R. Osellame, R. Ramponi, V. Giovannetti, R. Fazio, L. Sansoni, F. De Nicola, F. Sciarrino, and P. Mataloni, Anderson localization of entangled photons in an integrated quantum walk, Nat. Photonics **7**, 322 (2013).

[32] M. C. Rechtsman, J. M. Zeuner, Y. Plotnik, Y. Lumer, D. Podolsky, F. Dreisow, S. Nolte, M. Segev, and A. Szameit, Photonic Floquet topological insulators, Nature (London) **496**, 196 (2013).

[33] L. Lu, J. D. Joannopoulos, and M. Soljačić, Topological photonics, Nat. Photonics **8**, 821 (2014).
[34] S. Barkhofen, T. Nitsche, F. Elster, L. Lorz, A. Gabris, I. Jex, and C. Silberhorn, Measuring topological invariants and protected bound states in disordered discrete time quantum walks, Phys. Rev. A **96**, 033846 (2017).
[35] M. Z. Hasan and C. L. Kane, Colloquium: topological insulators, Rev. Mod. Phys. **82**, 3045 (2010).
[36] X. L. Qi and S. C. Zhang, Topological insulators and superconductors, Rev. Mod. Phys. **83**, 1057 (2011).
[37] S. Ryu, A. P. Schnyder, A. Furusaki, and A. W. W. Ludwig, Topological insulators and superconductors: Ten-fold way and dimensional hierarchy, New J. Phys. **12**, 065010 (2010).
[38] J. C. Y. Teo and C. L. Kane, Topological defects and gapless modes in insulators and superconductors, Phys. Rev. B **82**, 115120 (2010).
[39] W. Hu, J. C. Pillay, K. Wu, M. Pasek, P. P. Shum, and Y. D. Chong, Measurement of a Topological Edge Invariant in A Microwave Network, Phys. Rev. X **5**, 011012 (2015).
[40] S. Mittal, S. Ganeshan, J. Fan, A. Vaezi, and M. Hafezi, Measurement of topological invariants in a 2D photonic system, Nat. Photon. **10**, 180 (2016).
[41] J. M. Zeuner, M. C. Rechtsman, Y. Plotnik, Y. Lumer, S. Nolte, M. S. Rudner, M. Segev, and A. Szameit, Observation of a Topological Transition in the Bulk of a Non-Hermitian System, Phys. Rev. Lett. **115**, 040402 (2015).
[42] J. K. Asbóth and H. Obuse, Bulk-boundary correspondence for chiral symmetric quantum walks, Phys. Rev. B **88**, 121406 (2013).